

Study of Ordering and Properties in Fe-Ga Alloys With 18 and 21 at. pct Ga

IGOR S. GOLOVIN, L.YU. DUBOV, YU.V. FUNTIKOV, V.V. PALACHEVA, J. CIFRE, and D. HAMANA

Dynamical mechanical and positron annihilation spectroscopies were applied to study the structure of two Fe-Ga alloys with 18 and 21 at. pct Ga after quenching and subsequent annealing. It was found that the alloy with 18 pct Ga has much better damping capacity ($\Psi \approx 30$ pct) than the alloy with 21 pct Ga ($\Psi \approx 5$ pct). The reason for that is the ordering of the Ga atoms in Fe-21Ga alloy. Ordering processes in both alloys are studied at heating by differential scanning calorimetry, dilatometry, and internal friction or by step-by-step annealing using positron annihilation spectroscopy and hardness tests. Experimental results are explained by sequence of ordering transitions: A2 \rightarrow D0₃ \rightarrow L1₂.

DOI: 10.1007/s11661-014-2721-3

© The Minerals, Metals & Materials Society and ASM International 2015

I. INTRODUCTION

FE-GA binary alloys or “Galfenol,” being known by their extremely high magnetostriction, are used as smart magnetostrictive materials for sensor and actuator applications.^[1] According to existing phase diagrams, ordering of Ga atoms in body-centered cubic (bcc) iron takes place: The type of order depends on the temperature and concentration of Ga atoms. In this article, we do not study magnetostriction in the binary Fe-Ga alloys: These results are broadly discussed in the literature (*e.g.*, References 2 and 3), but we focus on influence of structure on damping capacity of the alloys. According to the *equilibrium* Fe-Ga diagrams (Figure 1(a)), alloys with 11 and more pct Ga belong to a (A2 + L1₂) phase mixture. The formation of the equilibrium face-centered cubic (fcc)-based L1₂-ordered phase below 873 K (600 °C) is rather slow, and in many cases, the decomposition and ordering develop in accordance with the *metastable* phase diagram (Figure 1(b)) which suggests a mixture of A2 and D0₃ phases at room temperature.^[2] Quenching from the A2 range of diagram suppresses the formation of ordered structures in favor of the disordered A2 structure. Annealing of quenched samples produces a two-phase mixture of A2 + D0₃ phases.^[4]

The values of magnetostriction λ in Fe-Ga alloys are significantly higher than those in α -Fe (*e.g.*, for

Fe-17Ga: $\lambda_{100} = 207 \times 10^{-6}$, $\lambda_{111} = -12 \times 10^{-6}$, $\lambda_{\text{polyer}} \approx 76 \times 10^{-6}$).^[5] Compositions with around 19 pct Ga have reported strains of up to 400 ppm along the $\langle 100 \rangle$ direction with low saturation fields of several hundred oersteds.^[6] Magnetic domains with 90 deg and 180 deg domain walls, which are typical for soft magnetic materials with positive anisotropy energy, are the source for the high damping properties of these alloys.

An increase in Ga content in α -Fe up to 30 at. pct nonmonotonously increases magnetostriction (λ) of Fe-Ga alloys, which is responsible for their main functional properties. This dependence has two maxima at ~ 20 and ~ 28 at. pct Ga for quenched alloys (Figure 2 was adapted from Reference 3). The idea of this article is to study two Fe-Ga alloys, which belong to two different groups: (1) before and (2) after the first peak at the dependence “ λ vs pct Ga.” For the first group we choose alloys with 18 pct Ga, for the second group—with 21 pct Ga.

In this article, we use two relatively new methods for studying Fe-Ga alloys: positron annihilation spectroscopy and dynamical mechanical spectroscopy. We focus on studying frequency-, amplitude-, and temperature-dependent damping,^[7] and processes during annealing of as quenched samples by positron annihilation method^[8] with the support of differential scanning calorimetry (DSC), X-ray diffractometry (XRD), and hardness tests.

Positron annihilation lifetime spectroscopy (PALS) is widely used for detecting defects in various materials after mechanical and thermal treatment. This technique is a sensitive method to study open-volume-type defects, which include point defects (vacancies and vacancy agglomerates) and linear and planar defects (dislocations and grain boundaries). The positrons, which have high energy, thermalize and diffuse in the crystalline lattice after they have entered the alloy. A part of positrons annihilates with electrons in the defect-free lattice (bulk annihilation) and another part is trapped by different defects of crystalline lattice. The positrons trapped by defects are bound there until their annihilation.

IGOR S. GOLOVIN, Professor, and V.V. PALACHEVA, Student, are with the National University of Science and Technology “MISIS”, Leninsky Ave. 4, Moscow 119049, Russia. Contact e-mail: i.golovin@isis.ru L.YU. DUBOV, Senior Lecturer, is with National Research Nuclear University “MEPHI”, Kashirskoe Highway 31, Moscow 115409, Russia. YU.V. FUNTIKOV, Research Fellow, is with the RF SSC Institute for Theoretical and Experimental Physics, Bolshaya Cheremushkinskaya Str. 25, Moscow 117218, Russia. J. CIFRE, Research Assistant, is with the Universitat de les Illes Balears, Ctra. de Valldemossa, km.7.5, 07122 Palma de Mallorca, Spain. D. HAMANA, Professor, is with École Nationale Polytechnique, University Constantine, Ain El Bey Road, Constantine 25000, Algeria.

Manuscript submitted August 4, 2014.

Article published online January 15, 2015

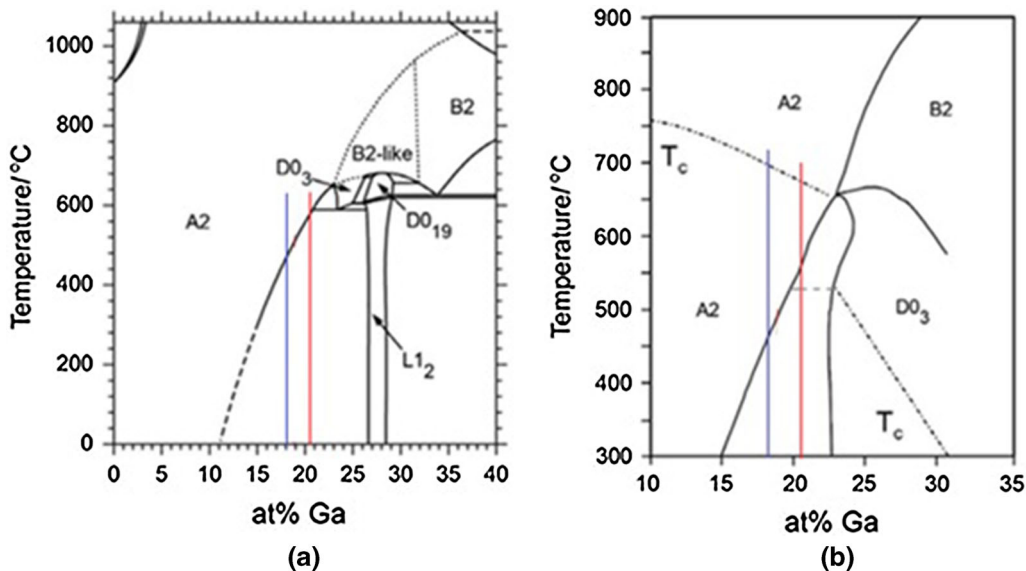


Fig. 1—Stable (a) and metastable (b) Fe-Ga phase diagrams adopted from Ref. [2]. The alloys studied in this article are shown in the diagrams.

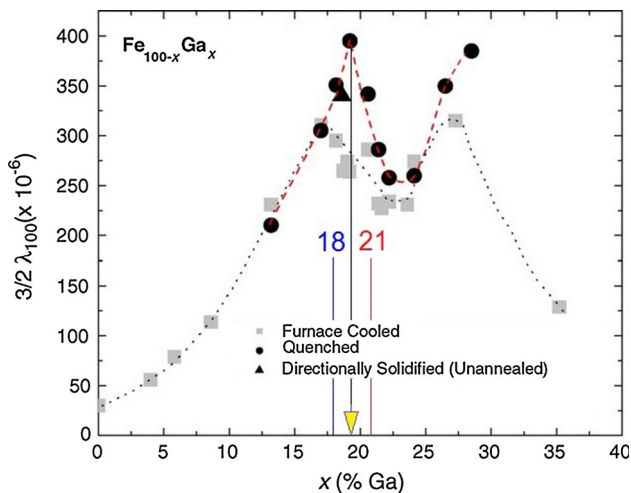


Fig. 2—Magnetostriction $(3/2)\lambda_{100}$, as a function of Ga in Fe-Ga alloys.^[3] The alloys studied in this article are shown in the diagram.

lation with electrons (trapping state annihilation). The measured positron lifetime is linked to the type of the defects and intensities of the lifetime spectrum components are related to the defect concentrations. Thus, it is possible to derive from the positron lifetime spectrum an information about the type of defects in the studied material and to evaluate their concentration.

II. EXPERIMENTAL PROCEDURE

Polycrystalline galfenols with a nominal composition $\text{Fe}_{82}\text{Ga}_{18}$ and $\text{Fe}_{79}\text{Ga}_{21}$ were prepared using commercially pure Fe and 99.999 pct pure Ga by induction melting in vacuum furnace. Then, the cast buttons were homogenized at 1373 K (1100 °C) for 20 minutes to eliminate the possible microsegregation, then forged and

rolled into a plate with a thickness of 2 mm. Using energy-dispersive spectroscopy (EDS), chemical compositions of the cast button were revealed to have an average compositions of Fe-18.3 at. pct Ga and Fe-20.5 at. pct Ga with accuracy within ± 0.3 pct.

The samples were cut from the plate using a cutting machine and underwent thermal treatments. The samples were annealed for 40 minutes at 1273 K (1000 °C) in a furnace, then they were cooled in water (*wq*—water quenching), and additionally several water quenched samples were annealed at different temperatures for 60 minutes. Consequently, the samples were denoted as $wq_{1273\text{ K}}$ ($wq_{1000\text{ °C}}$) and wq_{ann} samples.

Thermal analysis measurements were carried out using Labsys Setaram equipment with heating rates from 20 to 40 K/min. The microstructure of the samples was examined by X-ray diffractometer (XRD) using a Bruker D8 Advanced diffractometer (Bruker, <http://www.bruker.com/about-us.html>) with monochromatic Cu K α radiation. Hardness measurements were carried out using the universal hardness tester Wolpert 930N. The indentation force and the dwell time were set to 500g and 10s respectively. An average value of at least 10 individual measurements was used to characterize the microhardness.

Internal friction (IF, or Q^{-1}), *i.e.*, $\tan\varphi$ at forced vibrations, where φ is the phase lag between the applied cyclic stress and the resulting strain: $\sigma = \sigma_0 \cos(\omega t)$ and $\varepsilon = \varepsilon_0 \cos(\omega t + \varphi)$, correspondingly, where $\omega = 2\pi f$ and φ is the phase or loss angle, has been measured on a dynamical mechanical analyzer DMA Q800 (TA Instruments). These measurements were conducted as a function of temperature between 273 K and 873 K (0 °C and 600 °C), using forced bending vibrations in the range between 0.3 and 30 Hz with $\varepsilon_0 = 7 \times 10^{-5}$ with a heating and cooling rate of 1 K/min [temperature-dependent internal friction (TDIF) and temperature-dependent elastic modulus (TDEM)]. Additional measurements were conducted at room temperature

(RT) as a function of amplitude between 4×10^{-6} and 2×10^{-3} at a frequency of 3 Hz [amplitude-dependent IF (ADIF) and amplitude-dependent elastic modulus (ADEM), correspondingly] and as a function of frequency in the range from 0.01 to 200 Hz.

The positron lifetime measurements were performed at RT by means of a conventional fast-fast coincidence spectrometer. We employed a ^{22}Na β^+ -source of about 2 MBq and collected about two million counts for each sample. The positron lifetime is measured by detecting the time difference between the birth of nuclear γ -radiation of the ^{22}Na β^+ source and one of the annihilation γ -quanta with energy of 511 keV. The time resolution of the system is 230 ps.

The positron lifetime data were analyzed by using the PALSFIT program. After subtracting the source contribution, the multiexponential fit was applied. The experimental spectra were fitted by one and by three components. One component processing gives the average positron lifetime of the sample. Three components fit allows to allocate the contribution of defects. The shortest components were associated with the bulk annihilation, and the others were associated with the annihilation in the different trapping states. The positron trapping rates (k_{12} and k_{13}) were calculated from the intensities (I_2 and I_3) of trapping state components using the three state standard trapping model.^[9]

$$I_2 = \frac{k_{12}}{1/\tau_b - 1/\tau_2 + k_{12} + k_{13}}, \quad [1a]$$

$$I_3 = \frac{k_{13}}{1/\tau_b - 1/\tau_3 + k_{12} + k_{13}}, \quad [1b]$$

where τ_2 and τ_3 are the positron lifetimes for corresponding trapping states. The bulk lifetime for Fe-21Ga was evaluated as $\tau_b = 119$ ps. Then, the trapping rates derived from Eqs. [1a] and [1b] were used to estimate the defect concentration

$$C_x = k_{1x}/\mu_{1x} \quad [2]$$

where C_x is a defect concentration and the proportionality constant μ_x is the trapping coefficient for x -type defect. To estimate vacancy and linear defect density by Eq. [2], we used the positron trapping coefficients for single vacancy $\mu_{13} = \mu_v = 1.1 \times 10^{15} \text{ s}^{-1}$ ^[10] and the average trapping coefficient for dislocations ($\mu_{12} = \mu_{\text{dis}} = 0.6 \text{ cm}^2\text{s}^{-1}$) in pure α -Fe.^[11]

III. RESULTS

A. FDIF and FDEM

The test conditions for damping measurements were chosen according to the data shown in Figure 3, where typical frequency-dependent curve (maximal amplitude of deformation $\varepsilon_0 = 7 \times 10^{-5}$) is presented at room temperature for the Fe-21Ga sample. Dynamical mechanical analyzer (DMA Q800 TA Instruments)

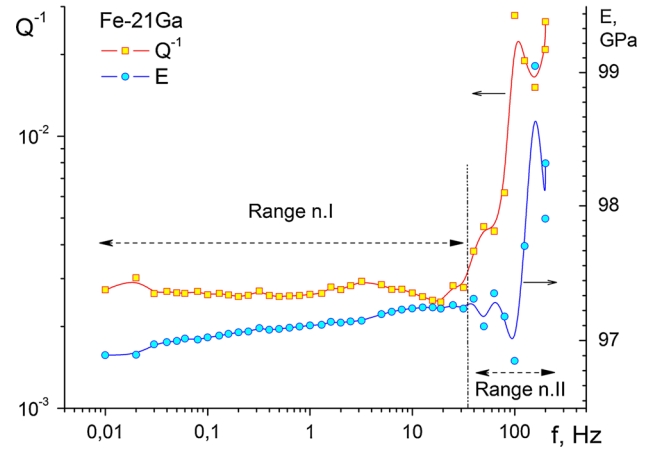


Fig. 3—Frequency-dependent internal friction: f varies from 0.01 to 200 Hz, $\varepsilon_0 = 0.007$ pct, $T = 303$ K (30 °C).

sweeps the frequency of forced vibrations in the range between 0.01 and 200 Hz.

B. ADIF

In Figure 4(a), one can see ADIF curves for different states of the alloy [measuring frequency is 3 Hz, temperature is 303 K (30 °C)]. An increase in testing temperature from 303 K to 573 K (30 °C to 300 °C) decreases damping and amplitude of damping peak at ADIF curves in agreement with a decrease in magnetization with temperature (Figure 4(b)).

C. TDIF and TDEM

Figure 5 shows TDIF and TDEM curves for Fe-18Ga (left column) and Fe-21Ga (right column) alloys water quenched from 1273 K (1000 °C). The heating and cooling rate of 1 K/min at maximal strain ε_0 equals 7×10^{-5} , and five chosen frequencies (see Section III–A) are used in the temperature range from 273 K to 873 K (0 °C to 600 °C). After heating to 873 K (600 °C), the samples were cooled to 273 K (0 °C) under the same measuring conditions.

There are some similarities between these two alloys: At heating, both alloys exhibit two frequency-dependent peaks at around 323 K to 373 K (50 °C to 100 °C) (denoted in this article as the P1 peak) and 423 K to 473 K (150 °C to 200 °C) (P2) followed by frequency-independent peak or peaks at 523 K to 673 K (250 °C to 400 °C) (P_{Ti}), and then again, a frequency-dependent peak at 723 K and 823 K (450 °C and 550 °C) (P3). Another frequency-independent peak is recorded at 848 K to 853 K (575 °C to 580 °C) at cooling of the furnace cooled sample (Figure 5(f)).

D. Heat Flow, Dilatometry, and XRD Tests of Water-Quenched Samples

The results of the heat flow and the dilatometry tests for $wq_{1273 \text{ K}}$ ($wq_{1000 \text{ °C}}$) samples are shown in Figure 6.

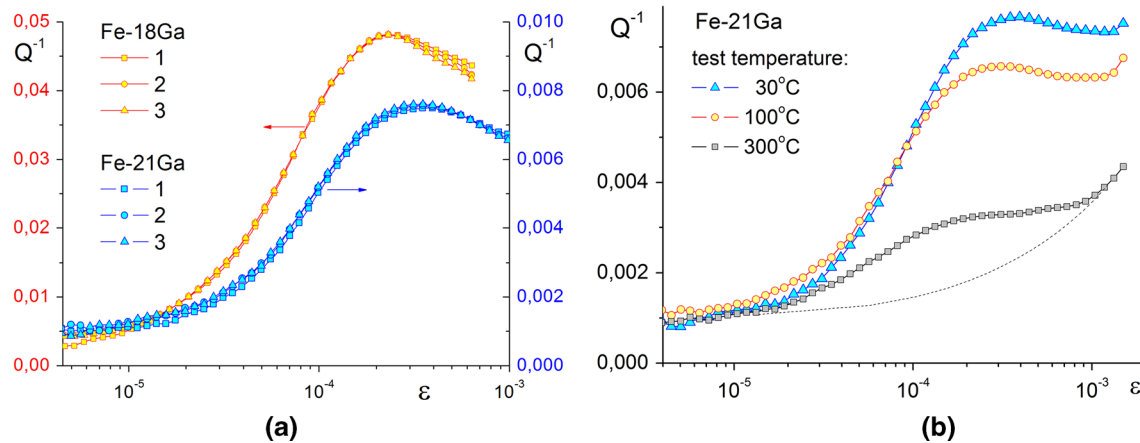


Fig. 4—Amplitude-dependent internal friction curves for Fe-18Ga and Fe-21Ga samples, $f = 3$ Hz, $T = 303$ K (30 °C): three tests for each sample (a). Amplitude-dependent internal friction curves for Fe-21Ga samples, $f = 3$ Hz, at different temperatures (b). The dotted black line is the extrapolation for the nonmagnetic background.

Below ~ 473 K (200 °C), a normal thermal expansion takes place. Between 473 K and 623 K (200 °C and 350 °C), there is a relative volumetric contraction at the dilatometry curve and an exothermal effect at the DSC curve. By approximating the DSC exothermal peak positions to zero heating rate, we get temperatures of about 513 K to 523 K (240 °C to 250 °C) for this effects in both alloys. XRD shows appearance of the $L1_2$ phase after annealing at 673 K (400 °C). After annealing at 573 K (300 °C), the $L1_2$ phase was not detected (Figure 7).

E. Positron Annihilation Lifetime Spectroscopy

To define the average positron lifetime in the sample, one component fit of the experimental spectrum is applied. Figure 8 shows the fitted average positron lifetime (τ_{av}) as a function of the isochronal annealing temperature (annealing time 60 minutes) and corresponding hardness of the samples. The positron lifetime spectrum for a sample quenched from 1273 K (1000 °C) consists of a single component with lifetime 175 ps. The average lifetime changes only a little from room temperature up to 473 K (200 °C) annealing temperature. For annealing temperature above 473 K (200 °C), a strong decrease of the lifetime occurs until a minimum is reached at 623 K (350 °C), for a value of $\tau_{av} = 155$ ps. At 673 K (400 °C) a sudden increase in τ_{av} takes place. Average lifetime returns to the initial value of 175ps at 773 K (500 °C). As one can see, the positron lifetime behavior correlates with variations in the hardness, which is related to the dislocation mobility.

Three-component fitting allows to estimate concentration of dislocations and monovacancies in the sample. The obtained dependence of the concentration on the annealing temperature is shown in Figure 9. The arrows at the ends of the vacancy curve indicate that the concentrations of vacancies at these points are beyond the dynamic range of the positron lifetime spectrometer, *i.e.*, greater than 5×10^{-4} vacancy per atom in the case.

IV. DISCUSSION AND CONCLUSIONS

Dynamical mechanical spectroscopy performed at frequencies above 30 to 40 Hz exhibits an artificial peak-like effect due to an unfortunate ratio of sample and apparatus stiffness, which leads to a resonance-like effect (Figure 3). At least from the viewpoint of absolute damping values and scattering of experimental points, damping measurements at frequencies higher than $f > 30$ Hz (range II in Figure 3) are not reliable. The increase in time for different relaxation processes in the alloy leads to a decrease in modulus and a weak increase in damping with lowering frequency in the range I. Nevertheless, tests at frequencies below 0.3 Hz are very time consuming. Usage of such low frequencies for temperature-dependent tests with a typical heating and cooling rate of 1 K/min leads to a too low density of experimental points. Thus, five frequencies, 0.3, 1, 3, 10, and 30 Hz, have been chosen for our temperature-dependent tests and $f = 3$ Hz for amplitude-dependent tests for a fixed temperature.

Amplitude-dependent tests performed at the frequency of 3 Hz demonstrate huge differences in damping capacity between these two alloys in favor of the Fe-18Ga alloy (Figure 4): The damping index for Fe-18Ga $\Psi = 2\pi Q_m^{-1} > 30$ pct. This difference seems to be higher than the corresponding difference in magnetostriction values (Figure 2). From the Smith and Birchak theory,^[12] the value of maximal hysteretic internal friction is described as:

$$Q_{hmax}^{-1} = 0.34k\lambda_S E / \pi\sigma_i (at\sigma_0 \approx \sigma_{max}) \quad [3]$$

where Q_{hmax}^{-1} is the maximum value of Q_h^{-1} in the ADIF curve, σ_i is the average residual internal stress, $k = 1$ is a constant characteristic of the shape of the hysteresis loop, and E is Young's modulus. Thus, from the theory, a direct proportionality between maximal damping and saturation magnetostriction should exist: $Q_{hmax}^{-1} = K \times \lambda_S$. A deviation from this simple law was already noticed in several papers, for example

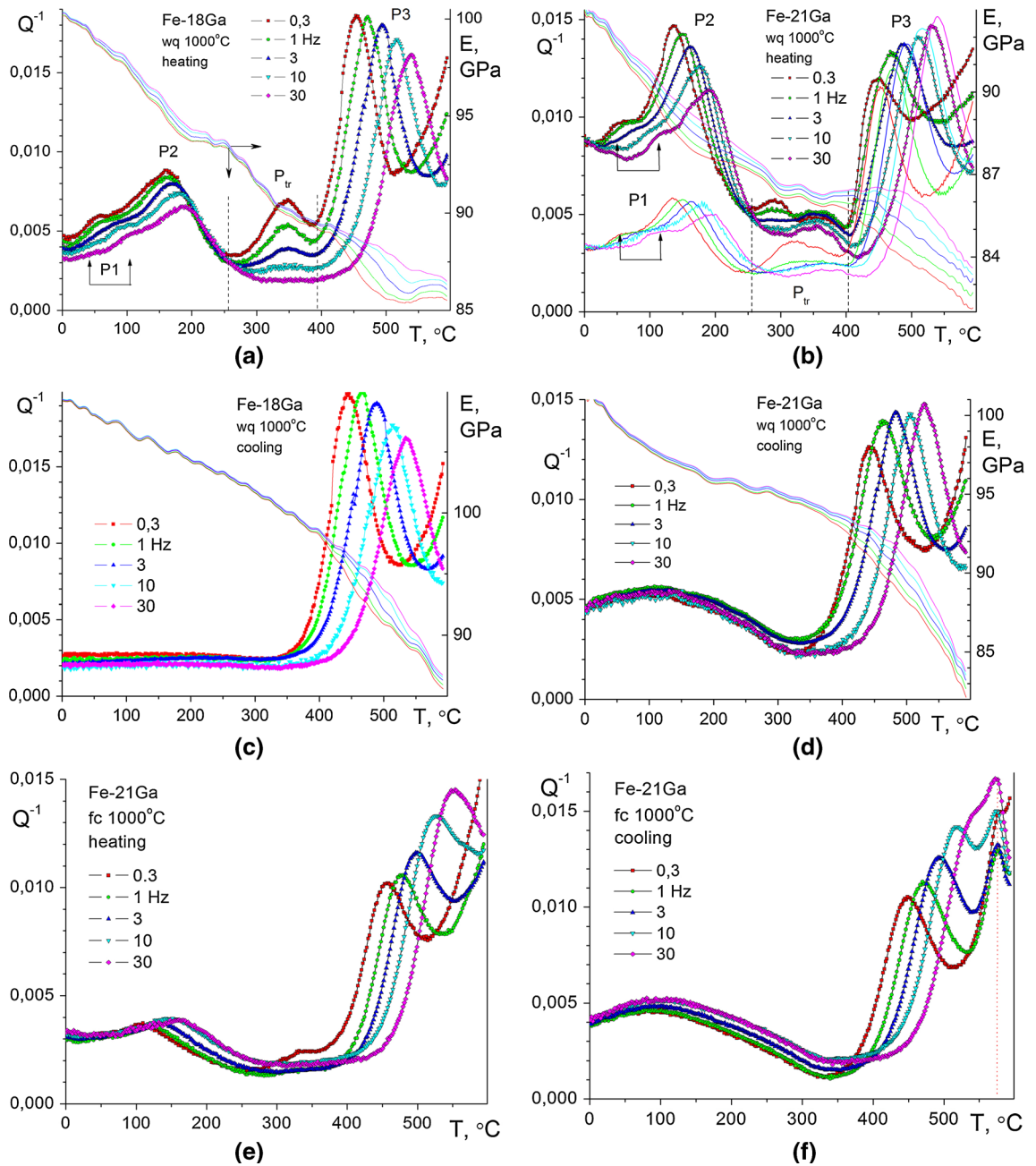


Fig. 5—Temperature-dependent internal friction curves for Fe-18Ga (a, c) and Fe-21Ga (b, d, e, f) samples after water quenching (a through d) and furnace cooling (e, f) from 1273 K (1000 °C) at heating (a, b, e) and subsequent cooling (c, d, f). The heating and cooling rate is 1 K/min. In Fig. 5(b), two TDIF tests are shown: directly after quenching (with experimental points) and after 1 month of natural aging (only lines). (a through d) Supplied with temperature dependencies of elastic modulus.

References 13 and 14. A similar sharp decrease in damping capacity was reported for Fe-Al alloys due to ordering of Al atoms in α -Fe.^[15,16]

Analyzing *temperature-dependent* internal friction peaks, we use the term “frequency dependent” to mean that a peak temperature depends on the frequency of vibrations; *i.e.*, the physical mechanism behind this effect is a thermally activated diffusion. Thus the peaks P1, P2, and P3 (Figure 5) are frequency dependent and their mechanism is controlled by thermally activated diffusion under applied cyclic stress. The peak temperature rises with the measurement frequency according to

the condition $\omega\tau = 1$ for a frequency-dependent Debye peak of internal friction represented by

$$Q^{-1} = \Delta \cdot \frac{\omega\tau}{1 + (\omega\tau)^2}, \quad [4]$$

where τ is the relaxation time and Δ is the relaxation strength. The temperature dependence of relaxation time controlled by thermally activated atomic jumps is described by an Arrhenius equation of the form

$$\tau^{-1} = \tau_0^{-1} \exp(-H/k_B T), \quad [5]$$

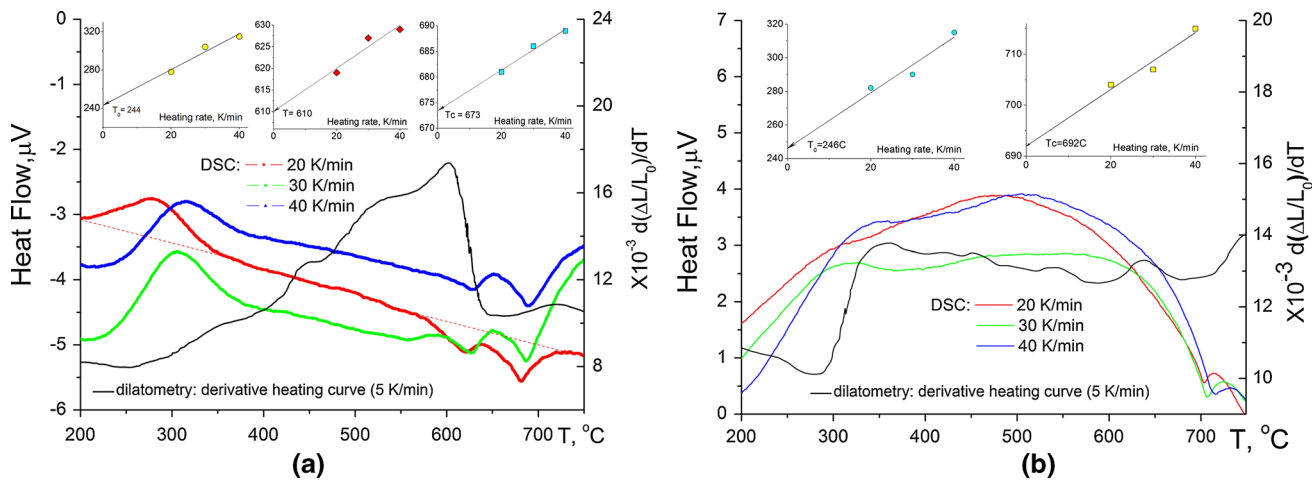


Fig. 6—Heat flow and derivation from dilatometry curve for $wq_{1273\text{ K}}$ ($wq_{1000\text{ °C}}$) Fe-21Ga (a) and Fe-18Ga (b) samples. Insets: approximation of peak temperatures to zero heating rate.

where H is the activation energy, τ_0 is the preexponential factor in the relaxation time, and k_B is the Boltzmann factor. The activation parameters (mean value of activation energy H and pre-exponential factor of inverse frequency τ_0) for physical process can be calculated using a frequency–temperature shift of the peak in coordinates: $\ln(2\pi f)$ vs $1/T$.

At cooling from 873 K (600 °C), the P1 and P2 effects disappear. Internal friction background below 623 K (350 °C) in the Fe-18Ga alloy is flat, whereas a frequency-independent broad peak-like IF behavior is recorded in the Fe-21Ga sample. The second heating and cooling test of the same sample reproduces the results obtained at the first cooling well. Activation parameters for all frequency-dependent peaks (P1, P2, and P3 at the first heating and P3 at cooling and subsequent heating-cooling run) are calculated and collected in the Tables I and II.

It is not easy to interpret the activation parameters generalized in Table I. In our earlier papers,^[14,17–19] we have concluded that the main contribution to the relaxation process between room temperature and 423 K (150 °C) in Fe-(8-13)Ga alloys comes from the Snoek-type effect, *i.e.*, from carbon atoms diffusion in solid solution under applied cyclic stress. Indeed, we did not record any thermally activated peaks in an interstitial free Fe-19Ga alloy.^[20] In contrast, a broad thermally activated peak with strange activation parameters has been recorded in several Fe-18(Ga + Al) alloys.^[14]

The current results allow to distinguish two peaks (P1 and P2) in the same temperature and frequency range (Figure 5). The activation parameters for the P1 peak, determined with rather low accuracy, suggest that this effect can be caused by both interstitial atoms and dislocation. We added carbon (0.07 at. pct) to Fe-18Ga alloy to enhance the Snoek type effect, but the response was not clear enough: Indeed, total damping in Fe-18Ga-C was increased mainly due to the rise in the internal friction background, but not the P1 and P2 peaks themselves. On the other hand, addition of 0.5 pct B instead of C pronouncedly decreases the P1 and P2

peaks, leaving the P3 peak unchanged. Considering the slow relaxation time ($\tau_0 = 10^{-12}$ to 10^{-13} seconds), the dislocation contribution to this effect is also possible. Nevertheless, the worm [573 K (300 °C)] drawing of the Fe-18Ga-B sample decreases both amplitude-dependent damping and the temperature-dependent damping in the vicinity of the P1 and P2 peaks similar to the influence of annealing of quenched samples.

There is a pronounced difference between the P2 peak parameters in the Fe-18Ga and the Fe-21Ga alloys. Activation parameters for a P2 peak—that looks thermally activated—are practically meaningless. The reason for obtaining these values is a structural transition, which takes place above 432 K (150 °C):^[14,17–20] this transition influences the peak shape and temperature.

The same conclusion had been made earlier for similar peaks in the Fe-18(Ga + Al) alloys.^[14] In fact, the P2 peak is a “pseudo” peak: It appears as the result of annealing processes. In the water-quenched Fe-Ga alloys, annealing processes include an annihilation of as-quenched vacancies (see details below) that contribute to formation of low-temperature internal friction background and an ordering of Ga atoms in α -Fe lattice.

The activation parameters for the P3 peak are rather reproducible and systematic; similar values were obtained in our earlier paper^[21] as well as for Fe-Ga alloys with different heat treatment and grain size.^[22] According to these parameters, the relaxation effect can be classified as the grain boundary relaxation.

Temperature for the P_{Tr} peak at 523 K to 673 K (250 °C to 400 °C) does not depend on vibrating frequency, whereas the height of this peak depends on frequency. We have to point out that if in the case of the Fe-18Ga alloy the data were well reproducible, then temperature-dependent spectra for the Fe-21Ga were slightly different, which might be the result of natural aging between quenching and tests. This aging may decrease vacancy concentration in the quenched sample. Nevertheless, the spectra are different in some details demonstrating the same general behavior. The results for two tests of the Fe-21Ga alloy, directly after

quenching (points) and 1 month after quenching (lines), are presented in Figures 5(b) and (d), respectively. Varying carbon and boron additions in the Fe-18Ga alloy has practically no effect on the P_{Tr} effect, whereas the addition of 5 pct Al decreases the P_{Tr} effect.

The P_{Tr} peak height is irreversibly proportional to measuring frequency: $Q_{Tr}^{-1} = A \times f^{-1}$, where the value A is proportional to a volume fraction of transition $\partial n / \partial T$. This dependence is typical for transient effects for displacive transformations^[23] and was already observed in several Fe-Ga-based alloys.^[14] If heating of a quenched sample is stopped at the temperature of the P_{Tr} peak maximum, then a decrease of IF takes place.

This effect is, most probably, caused by phase transition of the bcc-ordered $D0_3$ phase to the fcc-ordered $L1_2$ phase [523 K to 673 K (250 °C to 400 °C)], which is well recorded in Fe-21Ga alloy by XRD (Figure 7) and proved by structural studies in alloys with higher concentration of Ga.^[24] Even if this transition is, in general, diffusion controlled, then elements of a displacive shear transformation are involved. Namely, the loss of stability or buckling $\{110\}\langle 110 \rangle$ of the $D0_3$ phase takes place with formation of metastable

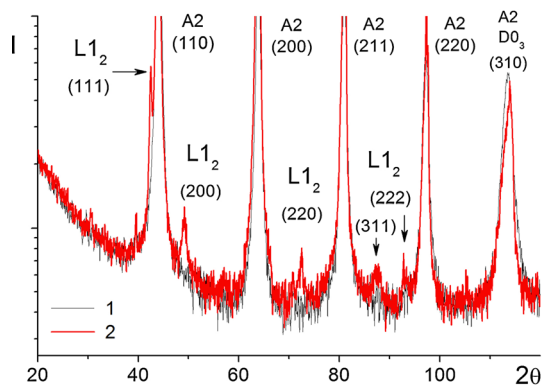


Fig. 7—XRD of water-quenched Fe-21Ga alloy after annealing at 573 K (300 °C) and 773 K (500 °C).

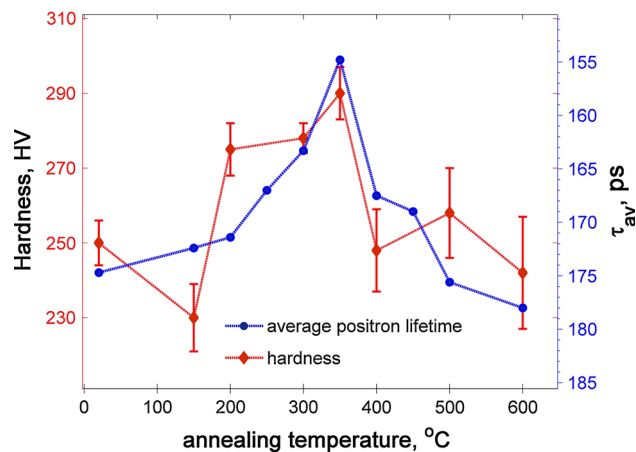


Fig. 8—The variations of average positron lifetime (τ_{av}) and hardness (HV) with annealing temperatures for $wq_{1273\text{ K}}$ ($wq_{1000\text{ °C}}$) Fe-21Ga samples.

closed-packed structure that is consistent with the Bain-type orientation relationship between bcc and fcc crystals. A similar viewpoint about displacive transformation or a stress-induced reorientation of tetragonal phase microdomains in Fe-Ga has been recently discussed by Khachatryan *et al.*^[25–27] The Bain strain is required for the diffusionless part of cubic to tetragonal displacive transformation that brings the structure closer to an equilibrium fcc-based $L1_2$ ordered phase. The features of the P_{Tr} peak are typical for shear transformations and thus can be associated only with this transformation in studied alloys.

The frequency-independent peak at 848 K (575 °C) at cooling of furnace-cooled sample (Figure 5(f)) is due to either order ($D0_3/L1_2$) \rightarrow disorder (A2) transition, or due to the eutectoid reaction $A2 + L1_2 \rightarrow D0_3$, which according to equilibrium phase diagram is at 861 K (588 °C) (Figure 1(a)). The alloy composition is very close to the boundary between these two reactions, which makes it difficult to separate.

To estimate the activation energy of a structural process between 423 K and 523 K (150 °C and 250 °C), which changes parameters of the P2 internal friction peak (heating rate 1 K/min), the exothermic heat flow peaks at 523 K to 623 K (250 °C to 350 °C) (heating rate from 20 to 40 K/min) were analyzed. Assuming that ordering of the supersaturated quenched Fe-Ga solid solution takes place and gives rise to exothermal DSC peak, tests with different heating rates were carried out and the Kissinger's^[28] method was used to calculate the activation energy of the ordered phase formation:

$$\ln \frac{\beta}{T_m^2} = -\frac{H_{act}}{RT_m} + C_2, \quad [6]$$

where β , T_m , and R represent the heating rate, the peak temperature, and the gas constant, respectively. The results are presented in Figure 6. The calculated values of activation energy of the $D0_3$ ordering process in Fe-18Ga and Fe-21Ga equal to 0.43 and 0.40 eV, correspondingly.

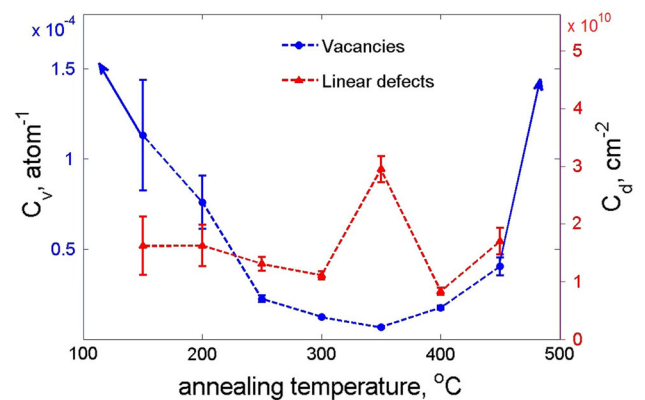


Fig. 9—The variations of vacancy (C_v) and linear (C_d) defects concentration with annealing temperatures for $wq_{1273\text{ K}}$ ($wq_{1000\text{ °C}}$) Fe-21Ga sample.

Table I. Activation Parameters for the P1 and P2 Relaxation Processes

| Heat Treatment | Peak 1 | | Peak 2 | |
|--|-----------------|-----------------------|-----------------|---------------------|
| | H (eV) | τ_0 (s) | H (eV) | τ_0 (s) |
| Fe-18Ga wq 1273 K (1000 °C), first test: heating | 0.79 ± 0.43 | 1.5×10^{-13} | 2.80 ± 0.81 | 3×10^{-34} |
| Fe-21Ga wq 1273 K, first test: heating | 0.72 ± 0.33 | 2.5×10^{-12} | 1.42 ± 0.06 | 2×10^{-18} |

Table II. Activation Parameters for the P3 Relaxation Process

| Heat Treatment | Heating | | Cooling | |
|----------------------------------|-----------------|-----------------------|-----------------|-----------------------|
| | H (eV) | τ_0 (s) | H (eV) | τ_0 (s) |
| | Fe-21Ga | | | |
| wq 1273 K (1000 °C), first test | 2.84 ± 0.02 | 7.8×10^{-21} | 2.69 ± 0.09 | 6.3×10^{-20} |
| wq 1273 K (1000 °C), second test | 2.69 ± 0.02 | 7.4×10^{-20} | 2.72 ± 0.06 | 4.1×10^{-20} |
| fc 1273 K (1000 °C), first test | 2.57 ± 0.02 | 8.2×10^{-19} | 2.47 ± 0.03 | 2.5×10^{-18} |
| fc 1273 K (1000 °C), second test | | | | |
| | Fe-18Ga | | | |
| wq 1273 K (1000 °C), first test | 2.87 ± 0.08 | 6×10^{-21} | 2.71 ± 0.09 | 6×10^{-20} |

Two endothermic peaks are recorded in Fe-21Ga alloy slightly above 883 K and 946 K (610 °C and 673 °C). Only one endothermic peak takes place in the Fe-18Ga alloy slightly above 966 K (693 °C). The above-mentioned temperatures are the result of the approximations of the temperatures at different heating rates to the zero heating rate (Figure 6, insets). The effects at 946 K and 966 K (673 °C and 693 °C) in Fe-18Ga and Fe-21Ga alloys are the Curie temperatures for disordered A2 solid solution. According to Reference 2, these Curie temperatures correspond to the composition of Fe-20.7Ga and Fe-19.0Ga. The effect at 883 K (610 °C) in the Fe-21Ga alloy is either due to order ($D0_3/L1_2$) \rightarrow disorder (A2) transition, or due to the eutectoid reaction $A2 + L1_2 \rightarrow D0_3$: Our alloy with 21 pct Ga is very close to the critical concentration above which this eutectoid reaction is possible. A big volumetric contraction between 873 K and 908 K (600 °C and 635 °C) (heating rate 5 K/min) takes place at the dilatometry curve most probably due to eutectoid reaction.

We do not see this reaction at IF spectra at heating because the upper limit for a temperature run is only 873 K (600 °C), but at cooling for a furnace cooled sample, we can see a frequency-independent peak at about 853 K (580 °C) (Figure 5(f)) due to the $D0_3 \rightarrow A2 + L1_2$ reaction.

Some additional information can be obtained from PALS tests. For the water-quenched state and after annealing at high temperatures 773 K to 873 K (500 °C to 600 °C), the one component fit of the experimental positron lifetime spectra is only appropriate. The lifetime of this component, 175 ps, is typical for monovacancies in iron.^[10] For other annealing temperatures, three components fit may be applied. The shortest lifetime τ_1 calculated using the trapping model corresponds to the evaluated bulk lifetime of Fe-21Ga

$\tau_b \approx 114$ ps. The most appropriate second lifetime $\tau_2 = 150$ ps is typical for linear defects^[11] and $\tau_3 = 175$ ps is the lifetime for monovacancies. So we can assume that the Fe-21Ga alloy contains at least two types of positron traps such as linear defects and single vacancies.

The water quenched from the 1273 K (1000 °C) Fe-21Ga sample contains a large number of single vacancies ($>5 \times 10^{-4}$ atom⁻¹). We suppose also that it contains a significant number of dislocations, but the concentration of vacancies is so high that we cannot see anything but them by PALS. After annealing at 423 K and 473 K (150 °C and 200 °C), the concentration of vacancies rapidly decreases and the dislocations become detectable. Dislocations are annealed slower than vacancies: Their density decreases slowly until 573 K (300 °C), and at 623 K (350 °C) a sudden increase is detected. It indicates that besides elimination of quenched dislocations, there is a generation of new defects with the positron lifetime close to the lifetime of linear defects in α -Fe. Such defects may arise as the result of phase transition at the antiphase boundaries $A2-D0_3$ or $D0_3-L1_2$, where the linear defects are formed to compensate for differences in the size of bcc-lattice $A2$, $D0_3$, and $L1_2$ phases. The process of new linear defects generation begins in the range between 473 K and 573 K (200 °C and 300 °C), and it is an additional sink for primary vacancies. At about 573 K (300 °C), there is a minimum of linear defects concentration; *i.e.*, the rates of elimination and generation become equal. At 623 K (350 °C), the maximum of linear defect and minimum of vacancy concentration is observed.

In the same temperature range, the increase in hardness and the P_{Tr} internal friction peak take place, reflecting the decrease of dislocation mobility and the appearing high density of the phase boundaries. A subsequent decrease of linear defect concentration after

annealing at 673 K (400 °C) may be the result of the coalescence of ordered phases, which becomes of a size of about 50 [annealing at 673 K (400 °C)], 100 nm [723 K (450 °C)], or 200 nm [773 K (500 °C)].^[2] The D₀₃ domains require formation of Ga-enriched particles inside the A2 phase in alloys with 18 or 21 pct Ga; thus, a large number of structural vacancies is necessary to compensate for the lack of Ga atoms. We observe an increase in the number of structural vacancies at annealing temperatures of more than 623 K (350 °C). The increase in the volume part of the D₀₃ domains leads to an increase in the vacancy concentration. Since the concentration of linear defects is proportional to the surface area of antiphase boundaries and the vacancy density is proportional to the volume of D₀₃ domains, it is logical to assume that between 573 K and 673 K (300 °C and 400 °C) the ratio of surface area of ordered nanodomains to their volume reaches a maximum and then decreases due to domain merger and appearance of the L₁₂ phase. From 673 K (400 °C), the rapid rise of thermal vacancy concentration takes place, and at an annealing temperature of 773 K (500 °C), we again go beyond the level of 5×10^{-4} vacancies per atom. This rise may be explained by increase of ratio volume/surface of D₀₃ domains and growth of L₁₂ phases.

To summarize the findings of this study:

- Water quenching of the Fe-18Ga alloy increases its intrinsic damping capacity as compared with furnace cooling or annealing of quenched sample. Damping capacity of water-quenched Fe-18Ga alloy ($\Psi \approx 30$ pct) is significantly higher than that in Fe-21Ga ($\Psi \approx 4.5$ pct).
- Analyses of temperature-dependent internal friction, heat flow and dilatometry tests and well as positron annihilation spectroscopy, XRD and hardness tests of water quenched Fe-Ga samples in step-by-step annealing regime, allows to conclude that two steps transition takes place: A2 \rightarrow D₀₃ ordering of Fe-Ga solid solution at 423 K to 573 K (150 °C to 300 °C) similarly to Fe-Al alloys^[30] and D₀₃ \rightarrow L₁₂ transition at 523 K to 723 K (250 °C to 450 °C). PALS tests indicate a generation of new defects at this stage with the positron lifetime close to the lifetime of linear defects in α -Fe. This transition sequence needs additional study by transmission electron microscope.
- Temperature-dependent internal friction curves of water-quenched samples exhibit a set of thermally activated and induced by structural transitions peaks. The activation parameters of these effects are calculated (Tables I and II) and hypothesis of their mechanisms are suggested: P1—point defects and dislocations motion, P2—beginning of the A2 \rightarrow D₀₃ transition and decrease in vacancies concentration, P_{Tr}—the D₀₃ \rightarrow L₁₂ transition, P3—grain boundary relaxation, P_{853 K} (P_{580 °C}) at cooling—D₀₃ \rightarrow A2 + L₁₂ reaction.

ACKNOWLEDGMENTS

The reported study was supported by RFBR (Russia) research project 14-03-00165a and Russian Federation State Task No. 1855. The authors are grateful to Dr. L.V. Elnikova for discussions.

REFERENCES

1. R.A. Kellogg, A.B. Flatau, A.E. Clark, M. Wun-Fogle, and T.A. Lograsso: *J. Appl. Phys.*, 2002, vol. 91, p. 7821.
2. O. Ikeda, R. Kainuma, I. Ohnuma, K. Fukamichi, and K. Ishida: *J. Alloy. Compd.*, 2002, vol. 347, p. 198.
3. T.A. Lograsso and E.M. Summers: *Mater. Sci. Eng. A*, 2006, vol. 416, pp. 240–45.
4. H. Cao, F. Bai, J. Li, D.D. Viehland, T.A. Lograsso, and P.M. Gehring: *JALCOM*, 2008, vol. 465, pp. 244–49.
5. M. Ishimoto, H. Numakura, and M. Wuttig: *Mater. Sci. Eng. A*, 2006, vol. 442, pp. 195–98.
6. A.E. Clark, K.B. Hathaway, M. Wun-Fogle, J.B. Restorff, T.A. Lograsso, V.M. Keppens, G. Petculescu, and R.A. Taylor: *J. Appl. Phys.*, 2003, vol. 93, p. 8621.
7. M.S. Blanter, I.S. Golovin, H. Neuhäuser, and H.-R. Sinning: *Internal Friction in Metallic Materials. A Handbook*, Springer, Berlin, 2007.
8. R. Krause-Rehberg and H.S. Leipner: *Positron Annihilation in Semiconductors*, Springer, Berlin, 1999.
9. B. Bergersen and M. Stott: *J. Solid State Commun.*, 1959, vol. 7, p. 1203.
10. A. Vehanen, P. Hautojärvi, J. Johansson, J. Yli-Kaupilla, and P. Moser: *Phys. Rev.*, 1982, vol. 25, p. 762.
11. Y.-K. Park, J.T. Waber, M. Meshii, C.L. Snead, Jr, and C.G. Park: *Phys. Rev. B*, 1986, vol. 34, p. 823.
12. G.W. Smith and J.R. Birchak: *J. Appl. Phys.*, 1968, vol. 39 (5), pp. 2311–15.
13. B. Astie and J. Degauque: *J. Physique. Colloq.*, 1983, vol. 44, no. C-9, pp. 461–70.
14. I.S. Golovin, V.V. Palacheva, V.Yu. Zadorozhnyy, J. Zhu, H. Jiang, J. Cirfe, and T.A. Lograsso: *Acta Mater.*, 2014, vol. 78, pp. 93–102.
15. V.A. Udovenko, S.I. Tishaev, and I.B. Chudakov: *Phys. Doklady*, 1993, vol. 38, pp. 168–76.
16. I.S. Golovin, H. Neuhäuser, A. Rivière, and A. Strahl: *Intermetallics*, 2004, vol. 12 (2), pp. 125–50.
17. I.S. Golovin and A. Rivière: *Intermetallics*, 2011, vol. 19, pp. 453–59.
18. I.S. Golovin, Z. Belamri, and D. Hamana: *J. Alloy. Compd.*, 2011, vol. 509, pp. 8165–70.
19. I.S. Golovin and J. Cifre: *J. Alloy. Compd.*, 2014, vol. 584, pp. 322–26.
20. A.A. Emdadi, J. Cifre, O.Yu. Dementeva, and I.S. Golovin: *J. Alloy. Compd.*, 2015, vol. 619, pp. 58–65.
21. I.S. Golovin: *Phys. Met. Metall.*, 2013, vol. 114 (12), pp. 1018–30.
22. M. Fang, J. Zhu, I.S. Golovin, J. Li, C. Yuan, and X. Gao: *Intermetallics*, 2012, vol. 29, pp. 133–39.
23. J. San Juan and R.P. Perez-Saez: *Mechanical Spectroscopy Q-1 2001 with Applications to Materials Science*, Eds. R. Schaller, G. Fantozzi, and G. Gremaud, Trans Tech Publications, Pfaffikon, Switzerland, 2001, pp. 416–37.
24. I.S. Golovin, V.V. Palacheva, A.A. Emdadi, M.Yu. Zadorozhnyy, A.V. Pozdnyakov, A.I. Bazlov, and S.A. Golovin: Unpublished research, 2014.
25. J. Boisse, H. Zapolsky, and A.G. Khachatryan: *Acta Mater.*, 2011, vol. 59, pp. 2656–68.
26. A.G. Khachatryan and D.D. Viehland: *Metall. Mater. Trans. A*, 2007, vol. 38A, pp. 2308–16.
27. A.G. Khachatryan and D.D. Viehland: *Metall. Mater. Trans. A*, 2007, vol. 38A, pp. 2317–28.
28. H.E. Kissinger: *Anal. Chem.*, 1957, vol. 29, pp. 1702–06.
29. Y.-K. Park, J.T. Waber, M. Meshii, C.L. Snead, Jr, and C.G. Park: *Phys. Rev. B*, 1986, vol. 34, p. 823.
30. I.S. Golovin, T.V. Pozdova, N.Ya. Rokhmanov, and D. Mukherji: *Metall. Mater. Trans. A*, 2003, vol. A34, pp. 255–66.